

Coupled multiscalar field dark energy

J. Alberto Vázquez^{1,*} David Tamayo^{2,†} Gabriela Garcia-Arroyo^{1,‡} Isidro Gómez-Vargas^{1,§}
Israel Quiros^{3,||} and Anjan A. Sen^{4,¶}

¹*Instituto de Ciencias Físicas, Universidad Nacional Autónoma de México,
62210, Cuernavaca, Morelos, México*

²*Instituto Tecnológico de Piedras Negras,*

Calle Instituto Tecnológico 310, C.P. 26080, Piedras Negras, Mexico

³*Departamento Ingeniería Civil, División de Ingeniería, Universidad de Guanajuato,
Guanajuato, C.P. 36000, México*

⁴*Centre for Theoretical Physics, Jamia Millia Islamia, New Delhi-110025, India*



(Received 26 May 2023; accepted 22 November 2023; published 10 January 2024)

The main aim of this paper is to present the multiscalar field components as candidates for the dark energy of the Universe and their observational constraints. We start with the canonical quintessence and phantom fields with quadratic potentials and show that a more complex model should satisfy current cosmological observations. Then, we present some implications for a combination of two fields, called quintom models. We consider two types of models: one as the sum of the quintessence and phantom potentials, and one including an interacting term between fields. We find that adding one extra degree of freedom, via the interacting term, enriches the dynamics considerably and could lead to an improvement in the fit of $-2 \ln \Delta \mathcal{L}_{\max} = 5.19$ compared to Λ CDM. The resultant effective equation of state is now able to cross the phantom divide line and in several cases presents an oscillatory or discontinuous behavior, depending on the interaction value. The parameter constraints of the scalar field models (quintessence, phantom, quintom, and interacting quintom) are performed using cosmic chronometer, type Ia supernovae, and baryon acoustic oscillation data, and the log-Bayes factors are computed to compare the performance of the models. We show that single scalar fields may face serious trouble and hence more complex models, i.e., multiple fields are necessary.

DOI: [10.1103/PhysRevD.109.023511](https://doi.org/10.1103/PhysRevD.109.023511)

I. INTRODUCTION

The current accelerated cosmic expansion is supported by multiple observations such as type Ia supernovae, the distribution of large-scale structure, the cosmic microwave background anisotropies (CMB), and the baryon acoustic oscillation (BAO) peaks; see [1,2] and references therein. These measurements may be an indication of a negative-pressure contribution to the total energy density of the Universe as being responsible for the accelerated expansion, commonly known as dark energy. Among numerous candidates that play the role of dark energy, the simplest and most well known is the cosmological constant term (Λ) introduced into the Einstein field equations, whose main features are that it has a constant energy density in time and is uniformly distributed in space. The cosmological

constant, along with cold dark matter, are the key elements that constitute the standard cosmological model or Λ CDM. Some of the essential properties to understand the nature of dark energy are encapsulated in its equation of state (EoS); for a barotropic perfect fluid, it is defined as the ratio of the pressure over its energy density, $w = p/\rho$. In particular, the Λ CDM model, having a dark energy EoS $w = -1$, describes most of the observational data very accurately; however, in recent studies it has seemed to display a tendency in favor of a time-evolving dark energy EoS $w(z)$ [3–8]. Therefore, several dark energy models with departures from the basic standard model have been introduced to take into account the evolution of $w(z)$, in addition to other properties [9]; for instance, single scalar fields have already been considered in cosmology to explain different phenomena, such as inflation, dark matter, and modified gravity, and they are also excellent candidates for modeling the variable dark energy EoS [3,10,11]. Two well-known single scalar fields (one degree of freedom) that have been extensively investigated for modeling dark energy are quintessence [12] and phantom dark energy [13]. Their Lagrangians have both a kinetic term and an associated potential, but the key distinction lies in the sign

*javazquez@icf.unam.mx

†david.tr@piedrasnegras.tecnm.mx

‡arroyo@icf.unam.mx

§igomez@icf.unam.mx

||iquiros@fisica.ugto.mx

¶aasen@jmi.ac.in

of their kinetic terms. The kinetic energy density for quintessence is positive, while that for phantom dark energy is negative. This slight difference results in distinct branches of values for their associated EoS parameter, i.e., for phantom dark energy $w < -1$ and for quintessence $-1 < w < 1$. Furthermore, the phantom divide line (PDL), defined as $w(z) = -1$, separates the phantom-energy-like behavior with $w < -1$ from the quintessence-like behavior with $w > -1$, and the existence of a no-go theorem shows that in order to cross the PDL at least two degrees of freedom are required for models (in four dimensions) involving ideal gases or scalar fields,¹ and this is where simple scalar fields may fail [15]. It is important to note that by using model-independent techniques or nonparametric approaches, i.e., artificial neural networks, Gaussian processes, or nodal reconstructions, multiple studies have shown a preference for a crossing of the PDL in the dark energy EoS parameter [4,6,16–19], which could also alleviate the Hubble tension and some inconsistencies among data sets, i.e., Ly- α and galaxy BAO data [20]. Following this line of research, different groups reconstructed the general form of $w(z)$ and converged on similar shapes [4,19,21]. If this trend continues in forthcoming experiments, single canonical scalar field models may face serious trouble and hence more complex theories or more than a single field would be needed to explain this important feature.

In order to model the richness of the evolution of $w(z)$, we need more than the usual quintessence/phantom dark energy and thus invoke more elaborate models. In [22] the authors constructed an EoS that crosses the PDL based on a two-field model. Within the scalar field scenario, a scalar field dark energy model with an EoS parameter that traverses the PDL during its evolution was first advocated and named quintom dark energy in [23]. Quintom dark energy is the next natural step for quintessence/phantom dark energy. This is a model that joins the quintessence and phantom fields (the reason behind its name) by considering both the positive and negative kinetic terms along with the potentials. Given that the null energy condition (NEC) is violated by the phantom degree of freedom [15], a quintom scenario is primarily designed for models with an NEC violation. The NEC-violating degree of freedom leads to a quantum instability and thus the fundamental origin of the quintom field poses a challenge for theoreticians. Nevertheless, if viewed just as an effective (classical) cosmological field, quintom models represent an interesting setup for PDL-crossing dark energy models. Quintom dark energy [24] has been studied from various perspectives, including theoretical aspects [25], observational constraints [26], dynamical systems approaches [20,27–29], nonminimal coupling [30], and quantum cosmology [31,32].

¹Bear in mind that for extra-dimensional models of dark energy, a single scalar field is able to cross the PDL [14].

Quintom models encompass interesting features of both quintessence and phantom dark energy: phantom dark energy has to be more fine-tuned than quintessence in the early Universe to serve as dark energy today, since its energy density increases with the expansion of the Universe; meanwhile, the quintom model mitigates the need for excessive fine-tuning by preserving—before the phantom domination—the tracking behavior of quintessence. Other research areas have also included similar ideas where two or more fields are present, such as two scalar fields or one field and its excited states as dark matter [33–36], a combination of the inflaton and scalar field dark matter [37], the presence of the inflaton and the curvaton field [38], two scalar fields to account for inflation [39,40], interactions between dark energy and dark matter [41], and the axiverse model [42–44] (see also [45]).

On the other hand, many investigations of model-independent techniques, along with current cosmological observations, have obtained a dynamical dark energy EoS and some of these results present wavering behaviors for the EoS, starting at $z = 0$ with $w < -1$, crossing the PDL, and then presenting a maximum and crossing back over the PDL, even multiple times. This type of model-independent behavior suggests the necessity to include two or more fields or to consider more complex potentials or even the coupling between these fields. A quintom model with an oscillating EoS was considered first in [46], starting from the idea of a wavering behavior. In this paper, we extend the work of single fields in [33] to multiple fields and revisit the quintom model with the addition of an interacting term, which may produce the oscillatory behavior and for some particular types of potentials can be justified by a symmetry group.

The paper is organized as follows. In Sec. II we summarize the main characteristics of the multiscalar field dark energy models. In Sec. III a novel quintom model with an interacting term is presented and we describe its main characteristics. In Sec. IV we present the data sets and statistical techniques used to constrain the cosmological parameters associated with the model. In Sec. V we present the main results. Finally, in Sec. VI we summarize our results and provide some comments and conclusions.

II. MULTISCALAR FIELD DARK ENERGY MODEL

In the context of four-dimensional spacetime, it is not feasible for a single scalar field to serve as a viable dark energy candidate for modeling the crossing of the phantom barrier. Therefore, it is necessary to introduce extra degrees of freedom, introduce nonminimal couplings, or modify Einstein's gravity. Adding extra degrees of freedom to the single scalar field dark energy requires the simultaneous consideration of more fields, as in the constructed quintom model which contains one canonical quintessence ϕ_1 and

one phantom ϕ_2 , and therefore the dark energy is attributed to their combination. The action of a cosmological model that incorporates multiple real scalar fields ϕ_i is given by

$$S = \int d^4x \sqrt{-g} \left[\frac{R}{2\kappa^2} + \frac{1}{2} \sum_i \epsilon_i \partial^\nu \phi_i \partial_\nu \phi_i - V(\vec{\phi}) + \mathcal{L}_M \right], \quad (1)$$

where $\kappa^2 = 8\pi G$ is the gravitational coupling and the term \mathcal{L}_M accounts for the remaining cosmological components of the Universe (dark matter, baryons, radiation, etc.). The index i represents the number of fields with a total associated potential $V(\vec{\phi}) = V(\phi_1, \dots, \phi_i)$, and the ϵ_i parameter is restricted to take either one of the two values $\epsilon_i = \{+1, -1\}$ in order to account for the distinction between quintessence (+1) and phantom (-1) fields, respectively.

Considering a flat Friedman-Robertson-Walker spacetime, the Friedmann equations are thus

$$H^2 = \frac{\kappa^2}{3} (\rho_Q + \rho_M), \quad (2)$$

$$\dot{H} = -\frac{\kappa^2}{2} (\rho_Q + p_Q + \rho_M + p_M), \quad (3)$$

where H represents the Hubble parameter and a dot denotes differentiation with respect to cosmic time. The standard energy density components $\rho_M = \sum \rho_j$, are assumed to be perfect fluids and have a barotropic EoS of the form $w_j = p_j/\rho_j$. Hence, the standard energy conservation equation for each one reads

$$\dot{\rho}_j + 3H(1 + \omega_j)\rho_j = 0. \quad (4)$$

In the case of pressureless matter we have $w_j = 0$, whereas for the relativistic particles $w_j = 1/3$. For the multifields, the associated total energy density and pressure are given by

$$\rho_Q = \frac{1}{2} \sum_i \epsilon_i \dot{\phi}_i^2 + V(\vec{\phi}), \quad p_Q = \frac{1}{2} \sum_i \epsilon_i \dot{\phi}_i^2 - V(\vec{\phi}), \quad (5)$$

and the EoS of the combined fields, i.e., the total effective EoS is then

$$w_Q = \frac{\sum_i \epsilon_i \dot{\phi}_i^2 - 2V(\vec{\phi})}{\sum_i \epsilon_i \dot{\phi}_i^2 + 2V(\vec{\phi})}, \quad (6)$$

whose value can only be determined from the evolution of the fields themselves. The dynamics of the scalar fields is determined by solving the following coupled Klein-Gordon equation:

$$\sum_i \left[\dot{\phi}_i \left(\epsilon_i \ddot{\phi}_i + 3H\epsilon_i \dot{\phi}_i + \frac{\partial V(\vec{\phi})}{\partial \phi_i} \right) \right] = 0. \quad (7)$$

For the particular case of $\phi_1 = \phi$ and $\phi_2 = \psi$, $\epsilon_1 = 1$ and $\epsilon_2 = -1$, and then $V = V(\phi, \psi)$ and thus the last expression becomes

$$\dot{\phi} \left(\ddot{\phi} + 3H\dot{\phi} + \frac{\partial V(\phi, \psi)}{\partial \phi} \right) - \dot{\psi} \left(\ddot{\psi} + 3H\dot{\psi} - \frac{\partial V(\phi, \psi)}{\partial \psi} \right) = 0. \quad (8)$$

In general, this equation does not enforce a split into two coupled Klein-Gordon equations; however, this specific splitting represents a special case where the overall equation is satisfied,

$$\ddot{\phi} + 3H\dot{\phi} + \frac{\partial V(\phi, \psi)}{\partial \phi} = 0, \quad (9)$$

$$\ddot{\psi} + 3H\dot{\psi} - \frac{\partial V(\phi, \psi)}{\partial \psi} = 0. \quad (10)$$

Clearly, the quintom model $\phi_1 = \phi, \phi_2 = \psi (\epsilon_1 = 1, \epsilon_2 = -1)$ boils down to quintessence when the phantom field is null, $\psi = 0$, and conversely into phantom dark energy when $\phi = 0$. In general, ϕ will evolve towards the local minima of the potential, whereas ψ evolves towards the local maxima; such different behaviors arise because of the signs in the Klein-Gordon equations, inherited from the signs of the kinetic energy terms in the action.

Finally, in order to determine the dynamics of the system, it is necessary to solve the conservation equations for the matter components and scalar fields. Following [33], the Klein-Gordon equations can be rewritten as a dynamical system that can be solved straightforwardly, where the initial conditions for each field are set up right into the matter domination epoch and we assume a thawing behavior for the multifields. This implies that at early times the kinetic terms of the quintom model vanish, and its equation of state w_Q begins at -1 . Also, the initial scalar field density parameter $\Omega_{Q, \text{ini}}$ is selected, through a shooting mechanism, such that its present value satisfies the Friedmann constraint, $\Omega_{Q,0} + \Omega_{M,0} = 1$. To illustrate the general behavior of the quintessence, phantom, and quintom models, in Fig. 1 we plot the following cosmological quantities: the EoS $w(z)$, Hubble function $H(z)$, Hubble distance D_H , and comoving angular distance D_M , along with several measurements (see the figure caption). In all panels, the Λ CDM model is represented by a black dashed line. As a proof of the concept, the potentials used in our analysis are as follows: for quintessence and phantom dark energy we use the quadratic potential, and for quintom we use the sum of the two aforementioned potentials,²

²For an ample variety of potentials, refer to [33].

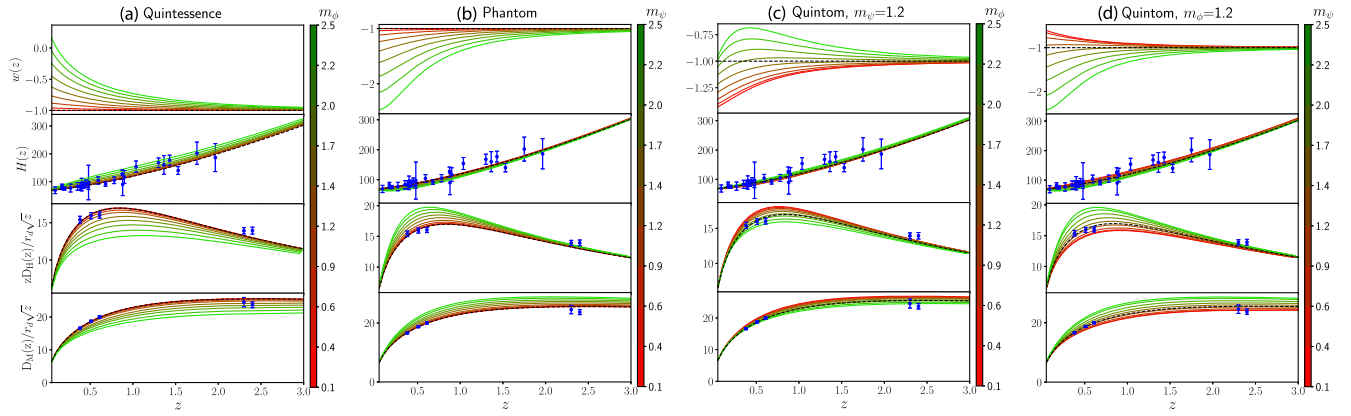


FIG. 1. From left to right: quintessence, phantom, and quintom cosmologies with potentials $V(\phi) = \frac{1}{2}m_\phi^2\phi^2$, $V(\psi) = \frac{1}{2}m_\psi^2\psi^2$, and $V(\phi, \psi) = \frac{1}{2}m_\phi^2\phi^2 + \frac{1}{2}m_\psi^2\psi^2$, respectively. The first row shows the EoS $w(z)$, the second row shows the Hubble function $H(z)$, the third row shows the Hubble distance D_H , and the fourth row shows the comoving angular distance D_M . The color bar represents different values for the masses of the fields. The data plotted for $H(z)$ correspond to the cosmic chronometers [48–55]; for the D_H and D_M panels we use the BAO galaxy consensus ($z \sim 0.5$) [56], Ly- α DR14 autocorrelation ($z = 2.34$), [57] and cross correlation ($z = 2.35$) [58]. In all panels, the black dashed line describes the Λ CDM model.

$$\text{quintessence: } V_\phi = \frac{1}{2}m_\phi^2\phi^2, \quad (11)$$

$$\text{phantom: } V_\psi = \frac{1}{2}m_\psi^2\psi^2, \quad (12)$$

$$\text{quintom: } V_\mathcal{Q} = \frac{1}{2}m_\phi^2\phi^2 + \frac{1}{2}m_\psi^2\psi^2. \quad (13)$$

Here m_ϕ, m_ψ are the masses of the fields, both of which are plotted in units of $[3H_0]$. To show the main behavior of the inclusion of the fields, we vary only the masses and keep the rest of the cosmological parameters fixed. Notice that, in general, for masses tending to null values we recover the Λ CDM pattern. In Figs. 1(a) and 1(b), the quintessence model shows an EoS $w > -1$, while for the phantom model $w < -1$. Notice that, in both cases, as the masses of the fields increase, the EoS deviates farther from the cosmological constant line ($w = -1$) in the late-time regime, but in opposite directions. In general, all of the quintessence $H(z)$ lines remain above the Hubble function of the Λ CDM model; this increment also allows D_H and D_M to lie below the Λ CDM model, but for the phantom model we see qualitatively opposite behavior. Both behaviors were already studied in [33]. On the other hand, for the quintom model and without losing generality, we consider two cases, shown in Figs. 1(c) and 1(d). In the first case, we fix the phantom mass at $m_\psi = 1.2$ and let the quintessence mass m_ϕ vary; in the second case, we reverse the scenario. For a fixed m_ψ [Fig. 1(c)], the PDL crossing occurs when $m_\phi \gtrsim m_\psi$, and depending on the ratio m_ϕ/m_ψ the dark energy EoS has a maximum that becomes more pronounced as m_ϕ/m_ψ increases; on the other hand, for a fixed m_ϕ the PDL crossing is less pronounced and the EoS may exhibit a minimum depending on the combination of

m_ψ/m_ϕ .³ Finally, in these last two cases, there is mixed behavior for $H(z)$, D_H , and D_M with regards to staying above or below the Λ CDM observables, depending on the mass-parameter combination. In all cases, the EoS converges to $w = -1$ at high redshift, by construction.

III. QUINTOM MODEL WITH INTERACTING TERM

The previous section presented a quintom model with a nondirect interacting term in the scalar field potential, i.e., it can be split into two independent functions of the fields $V(\phi, \psi) = V(\phi) + V(\psi)$; therefore, the Klein-Gordon equations (7) are coupled only through the Friedmann equation. Now, a next step is to consider a scalar potential with an interaction term. For a renormalizable model, a general form of the potential must include operators with dimension four or less, consisting of various powers of the scalar fields. A reasonable choice is to consider a potential that respects Z_2 symmetry, i.e., it is invariant under the following simultaneous transformations: $\phi \rightarrow -\phi, \psi \rightarrow -\psi$ [59]. A potential containing an interaction term between the fields ϕ and ψ and with the above properties has the following form⁴:

³In this work we focus on these type of models, named quintom-A fields, whose main feature is that at late times the phantom dominates ($w < -1$) where at early times the quintessence dominates ($w > -1$). However, it would be interesting to perform a similar analysis of its dual, a quintom-B field, that mirrors the EoS behavior along the PDL axis [47].

⁴This potential can also be derived from an inflaton-phantom unification protected by an internal $SO(1, 1)$ symmetry, with the two cosmological scalars appearing as the degrees of freedom of a sole fundamental representation [60,61].

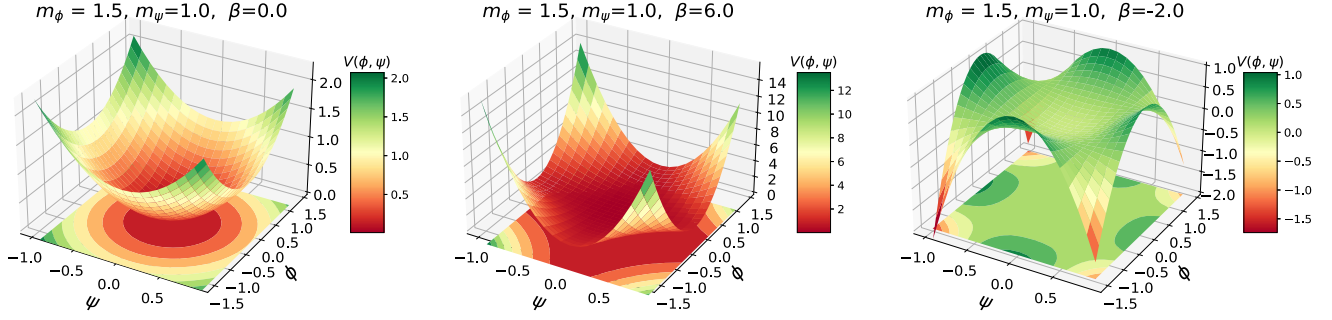


FIG. 2. Quintom potential (14) for fixed values of the masses and positive, null, and negative values of the coupling parameter β . The color bar indicates the values of the potential $V(\phi, \psi)$ (z axis).

$$V(\phi, \psi) = \frac{1}{2} m_\phi^2 \phi^2 + \frac{1}{2} m_\psi^2 \psi^2 + \beta \phi^2 \psi^2. \quad (14)$$

This is a particular case of the potential considered in Eq. (8) of Ref. [59] [see also Eq. (4) of Ref. [62]], where the authors set the mass-squared dimension's constant $\Lambda_0 = 0$ and make the identification $\lambda^2 = \beta$. Although phantom and quintom models, such as the one we are considering here [Eq. (14)], suffer from a severe problem of quantum instability [63,64], it has been argued that, since we are considering a classical theory of gravity (general relativity), these fields should only be considered as an appropriate effective description.

Due to the interaction term, $\beta \phi^2 \psi^2$, the equations of motion of the scalar fields are coupled, and hence the term related to the potential in the Klein-Gordon equation of the field ϕ becomes $\frac{\partial V(\phi, \psi)}{\partial \phi} = m_\phi^2 \phi + 2\beta \phi \psi^2 = f(\phi, \psi)$, which depends on both fields; the same happens for the ψ field. We refer to the quintom model with the potential (14) as the interacting quintom, or just “quintom + β .”⁵ Although the above potential was previously considered to describe the qualitative behavior of a cyclic universe [59,62], as far as we know, its observational consequences have not been previously investigated in detail. This is one of the reasons why we chose this specific quintom model for our study. The other reason, which has been already mentioned in the text, is that quintom models provide a feasible crossing of the phantom divide, a feature that seems to be favored by the observations.

Figure 2 displays the quintom + β potential for fixed values of the masses $m_\phi = 1.5$ and $m_\psi = 1.0$ and three values of the interaction constant $\beta = 0.0, 6.0, -2.0$. For the case $\beta = 0$, we recover the results of the previous section. For positive β there is a wide paraboloid with $V \geq 0$ whose minimum is in the region $\phi = \pm \frac{m_\psi}{m_\phi} \psi$, while in the negative β case the potential may get to negative values (seen in the color bar of the figure), which can be

⁵We base our analysis on this potential; however, in the Appendix there are some other interesting alternatives to explore in future works.

problematic as they may produce a negative energy density. However, such behavior has been studied throughout negative dark energy models [65–67] and a sign-switching cosmological constant Λ [68–71].

Let us explore some cosmological implications of the quintom + β model by numerically solving the full dynamical system. Similar to the previous cases, we compute the evolution of $w(z)$, $H(z)$, $D_H(z)$, and $D_M(z)$; their associated plots are shown in Fig. 3. In Fig. 3(a) (fixed $m_\psi = 1.2$, $\beta = 4.0$ and varying m_ϕ), the EoS at $w(z = 0)$ is in the phantom region, increases, and reaches a local/global maximum value. If the mass-ratio condition $m_\phi/m_\psi < 1$ is satisfied (red lines), then the effective field evolves only in the phantom region; however, for values $m_\phi \sim m_\psi$ it crosses to the quintessence regime, and in some combinations of the masses it is able to cross back into the phantom zone, therefore crossing the PDL twice. As the ratio m_ϕ/m_ψ increases (green lines), the maximum is shifted to larger redshifts and produces larger values of $w(z)$, and then remain in the quintessence region (the behavior of a quintom- Λ field, as mentioned previously). An interesting point to note is that the quintom + β model is able to traverse the Hubble Λ CDM line $H_{\Lambda\text{CDM}}(z)$ (black dashed line). That is, if $H_{\Lambda\text{CDM},0}$ is larger than the Hubble parameter given by the $H_{Q,0}$ of the quintom + β model, $H_{\Lambda\text{CDM},0} > H_{Q,0}$, then at some redshift it will occur that $H_{\Lambda\text{CDM}}(z) < H_Q(z)$. This type of behavior provides flexibility to transverse the Λ CDM observables $D_H(z)$ and $D_M(z)$, contrary to the decoupled quintom model [see Figs. 1(c) and 1(d)].

As the β parameter increases (and depending on the combination of the masses), the oscillation is more pronounced and the crossing of the Λ CDM observables is more notorious; see, for instance, Fig. 3(b) ($m_\phi = 1.2$, $\beta = 6.0$, and varying m_ψ). For $m_\psi/m_\phi < 1$ (red lines), the EoS presents a wavering behavior and crosses the PDL multiple times. As the ratio m_ψ/m_ϕ increases, there are fewer oscillations with smaller amplitudes, until the evolution becomes a fully phantom behavior (green lines). A similar oscillatory function of $w(z)$ has been found by using non-parametric reconstructions directly from observables [4] and in phenomenological models that encompass these

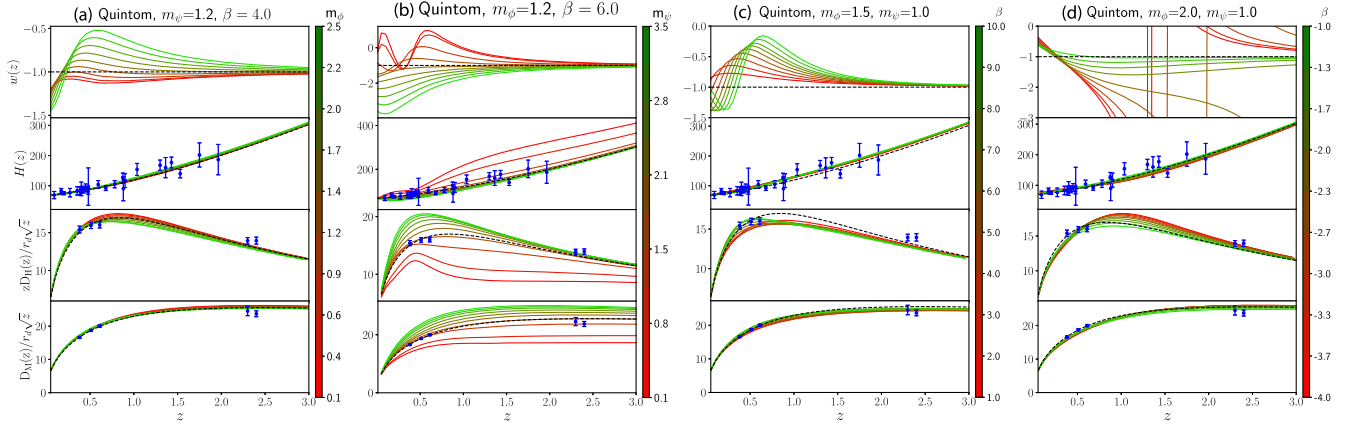


FIG. 3. Quintom model. Two of the three parameters (m_ϕ , m_ψ , and β) are fixed while the remaining varies in a range of values. From left to right, in the first panel we vary m_ϕ , in the second m_ψ , in the third $\beta \geq 0$, and in the fourth $\beta < 0$. The first row is the EoS $w(z)$, the second is the Hubble function $H(z)$, the third is the Hubble distance D_H , and the fourth is the angular distance D_M . The plotted data points are the same as in Fig. 1. The color bar represents different values for the masses of the fields or the β parameter.

features [72]. Figure 3(c) displays the outcomes for fixed mass values $m_\phi = 1.5$, $m_\psi = 1$ and taking only positive values of β . As the β parameter increases the wavering behavior is enhanced, and both the crossing of the PDL and the maximum value of the EoS shift to higher redshifts.

Finally, in Fig. 3(d) we show some peculiar behaviors when the negative case of β is taken into account; here we use $m_\phi = 2.0$ and $m_\psi = 1$. At the present time, $w(z)$ resides in the quintessence region, opposite to the $\beta \geq 0$ case, but in the past, it crosses the PDL and for high negative values of β the EoS diverges, to then come back to the quintessence region $w(z) > -1$ at early times. The presence of a pole in the EoS has been studied under several different physical circumstances in [65,68,73–79]. It is important to recall that $w(z)$ is not a physical observable, and thus its divergence does not imply a physical pathology or an obvious constraint or failure of the model. The origin of the pole is clear from the definition of the barotropic EoS, $w = p/\rho$, which occurs when the energy density of the quintom dark energy density turns out to be zero, i.e., when the negative terms of $\rho_Q = \frac{1}{2}(\dot{\phi}^2 - \dot{\psi}^2 + m_\phi^2\phi^2 + m_\psi^2\psi^2 - 2|\beta|\psi^2\phi^2)$ are relevant for certain values of β , such that $\rho_Q = 0$, and hence ρ_Q is able to change sign to become negative. A negative energy density can be associated with the sign of the cosmological constant, the hypothesis of a negative mass, or just an effective energy density similar to the curvature case; see, for instance, [66,69,80,81]. Regarding the Hubble function, we see opposite situation as in the previous cases. If $H_{\Lambda\text{CDM},0}$ is smaller than the Hubble parameter given by the quintom + β model $H_{Q,0}$, that is, $H_{\Lambda\text{CDM},0} < H_{Q,0}$, then at some redshift it occurs that $H_{\Lambda\text{CDM}}(z) > H_Q(z)$, and consequently the D_H and D_M cross from the bottom part to top part of the ΛCDM line, as seen in the lower panels of the same figure.

IV. CODE AND OBSERVATIONS

In this section, we perform the parameter estimation and provide observational constraints from the latest data on the free parameters of the quintessence, phantom, quintom, and quintom + β dark energy models considering the potentials (11)–(14), and discuss the model even further. In order to explore the parameter space, we use a modified version of DYNASTY, a library with several versions of the nested sampling algorithm. In conjunction, we utilize the SimpleMC cosmological parameter estimation code [82,83], which computes expansion rates and distances using the Friedmann equation to calculate the posterior distributions. Equipped with these tools, we can easily calculate the Bayesian evidence $\ln \mathcal{Z}$, an informative measure of the compatibility of the statistical model with the observed data, thereby allowing direct comparison of two cosmological models, a and b , using the Bayes factor $B_{ab} \equiv \mathcal{Z}_a/\mathcal{Z}_b$ or, equivalently, the relative log-Bayes evidence $\ln B_{ab} \equiv \Delta \ln \mathcal{Z}$. The model with the smaller $|\ln \mathcal{Z}|$ is the preferred model, and to interpret the results we refer to the Jeffreys scale: a weak evidence is indicated by $0 \leq |\Delta \ln \mathcal{Z}| < 1$, a moderate evidence by $1 \leq |\Delta \ln \mathcal{Z}| < 3$, a strong evidence by $3 \leq |\Delta \ln \mathcal{Z}| < 5$, and a decisive evidence by $|\Delta \ln \mathcal{Z}| \geq 5$, in favor of the model. For an extended review of cosmological parameter inference, see [84].

To perform the parameter estimation, we consider data from cosmic chronometers (HD), SNIa, and BAO measurements, which are detailed in the following list:

- (1) *HD*: Hubble distance measurements or cosmic chronometers are galaxies that evolve slowly and allow direct measurements of the Hubble parameter $H(z)$. We use the most recent compilation that contains a covariance matrix from Ref. [85].
- (2) *SN*: The SNIa data set used in this paper is Pantheon+, a compilation of 1550 SNIa within redshifts between $z = 0.001$ and $z = 2.26$ [86].

- (3) *BAO*: High-precision BAO measurements at different redshifts up to $z < 2.36$. We make use of the BAO data from the SDSS DR12 Galaxy Consensus, BOSS DR14 quasars (eBOSS), Ly- α DR16 cross correlation, Ly- α DR16 autocorrelation, Six-Degree Field Galaxy Survey, and SDSS Main Galaxy Sample [87].

Throughout the analysis, we assume a flat Friedmann-Lemaître-Robertson-Walker universe, and flat priors over our sampling parameters: $\Omega_{m0} = [0.05, 1.0]$ for the pressureless matter density parameter today, $\Omega_{b0}h^2 = [0.02, 0.025]$ for the physical baryon density parameter, and $h = [0.4, 1.0]$ for the reduced Hubble constant; in addition to these parameters, for the quintom model we have the quintessence field mass $m_\phi = [0.0, 4.0]$, the phantom field mass $m_\psi = [0.0, 3.0]$, and the coupling parameter $\beta = [-10.0, 10.0]$, but when using the combination of all data sets (BAO + HD + SN) we use $\beta = [-2.0, 4]$.

V. RESULTS

The main results of our analysis are shown in Table I where we report the constraints of the model parameters Ω_m , h , m_ϕ , m_ψ , β along with the 68% CL, for all different combinations of the data sets: HD, SN, BAO, HD + SN, BAO + HD, BAO + SN, and BAO + HD + SN. We also include the results of Λ CDM as the reference model. Additionally, the same table displays the best fit, $-2 \ln \mathcal{L}_{\max}$, along with the log-Bayesian evidence, $\ln \mathcal{Z}$, from the nested sampling algorithm, with the number of live points selected using the general rule $50 \times ndim$ [88], where $ndim$ is the number of parameters to be sampled from. Complementary to the table, in Figs. 4 and 5 we display the two-dimensional marginalized distributions (the inner and external contours are for the 68% and 95% CL, respectively) and the constraints in the form of one-dimensional marginalized posterior distributions: Fig. 4 corresponds to quintessence and phantom dark energy, and Fig. 5 corresponds to the quintom and quintom + β models; in both cases, we include the combination of data sets that provided the most constraining power.

In general, and among data sets, the quintessence and phantom models are statistically consistent with Λ CDM; however, there are some important points to mention. The quintessence model presents a nearly negligible improvement to describe data sets, that is, the comparison relative to the reference model⁶ is small, $-2 \ln \Delta \mathcal{L}_{\max} \lesssim 1$, except when both BAO and SN appear in the combined data set; for these combinations, the improvement of the fit yield $-2 \ln \Delta \mathcal{L}_{\max} \leq 2.85$. This can be understood by the lower m_ϕ values, which are accompanied by distinguishable

values of h compared to their counterpart in the Λ CDM model. Additionally, from the left panel of Fig. 4 it is evident that these data sets impose the tightest parameter constraints. Notice that the HD + SN combination gives the lowest m_ϕ value; nevertheless, for this reason, it is more capable of mimicking Λ CDM, having a slightly different change in h and a very similar fit. Consequently, the advantage of the additional parameter is lost. From the calculation of the Bayesian evidence, we can interpret that while Λ CDM is preferred over the quintessence model, this preference is generally weak for most of the data sets. However, for SN and HD + SN, the evidence in favor of Λ CDM is definite but not strong.

In contrast to the quintessence model, the phantom model exhibits a positive correlation between h and m_ψ when considering the BAO and extra data; see the left panel of Fig. 4. However, in this model the value of $-2 \ln \Delta \mathcal{L}_{\max}$ does not show improvement compared to Λ CDM, even when for BAO + SN and BAO + HD + SN the constraints on the scalar field mass are more restrictive than that found for quintessence. Analyzing the Bayesian evidence suggests that while the phantom model can be weakly or definitely less favored than Λ CDM, there is an exception for the HD sample, where it is indeed weakly favored. Notably, in this instance the parameter adjustment for m_ψ exhibits the biggest value for this model.

On the other hand, when the two fields are incorporated into the quintom model, notice that with the inclusion of the BAO data there is a positive correlation among the masses of the fields, but the correlation of the individual masses with the Hubble parameter is essentially lost (see the left panel of Fig. 5). For all data combinations, the parameter adjustments favor $m_\phi > m_\psi$, indicating that the quintom model prefers to be dominated by the quintessence branch. Similar to the quintessence model, the fit is improved when the BAO and SN data appear in the data set; in these cases, $-2 \ln \Delta \mathcal{L}_{\max} \leq 3.58$, and their corresponding h value is lower than that obtained for Λ CDM. However, the penalty carried by the extra parameters is more evident when analyzing the Bayes factors. According to this criterion, it is notable that when only HD data is employed, both models have the same Bayes factor and then both are equally favored. For the BAO and BAO + HD combination, the quintom model is weakly disfavored compared to the standard model. Furthermore, for the remaining data combinations, the preference over Λ CDM is enhanced and now definitive. It is worth nothing that under the Bayesian evidence, even the BAO + SN and BAO + HD + SN combinations, which previously seemed to provide better fits, are now disfavored.

Now let us focus on the novel model, quintom + β . The first point to highlight is that the β parameter is bounded by the different data sets, and even though the BAO and its combinations indeed provide tight constraints, with a slight preference for positive values of β , except for the SN data,

⁶Throughout the results we use Λ CDM as the reference model to compare with model i ; thus, $-2 \ln \Delta \mathcal{L}_{\max} \equiv -2 \ln(\mathcal{L}_{\Lambda\text{CDM,max}}/\mathcal{L}_{i,\text{max}})$.

TABLE I. Constraints at 68% CL on the parameters, $-2 \ln \mathcal{L}_{\max}$, and log-Bayesian evidence $\ln \mathcal{Z}$ for the quintessence, phantom, quintom, and quintom + β models, using different data sets.

Parameter	Data sets	Quintessence	Phantom	Quintom	Quintom + β	Λ CDM
Ω_m	HD	0.362 ± 0.120	0.346 ± 0.100	0.332 ± 0.103	0.346 ± 0.117	0.368 ± 0.108
	SN	0.306 ± 0.032	0.347 ± 0.026	0.309 ± 0.044	0.354 ± 0.083	0.332 ± 0.018
	BAO	0.300 ± 0.021	0.285 ± 0.020	0.276 ± 0.030	0.256 ± 0.033	0.292 ± 0.019
	HD + SN	0.311 ± 0.029	0.346 ± 0.024	0.311 ± 0.045	0.314 ± 0.084	0.332 ± 0.018
	BAO + HD	0.300 ± 0.019	0.287 ± 0.018	0.276 ± 0.030	0.252 ± 0.029	0.292 ± 0.018
	BAO + SN	0.300 ± 0.016	0.315 ± 0.014	0.296 ± 0.018	0.295 ± 0.018	0.313 ± 0.014
	BAO + HD + SN	0.301 ± 0.015	0.314 ± 0.014	0.298 ± 0.016	0.297 ± 0.016	0.312 ± 0.013
h	HD	0.630 ± 0.062	0.723 ± 0.083	0.722 ± 0.089	0.723 ± 0.088	0.661 ± 0.057
	SN	0.755 ± 0.162	0.737 ± 0.166	0.800 ± 0.141	0.671 ± 0.173	0.699 ± 0.174
	BAO	0.652 ± 0.048	0.739 ± 0.050	0.707 ± 0.074	0.747 ± 0.073	0.699 ± 0.022
	HD + SN	0.677 ± 0.040	0.674 ± 0.038	0.677 ± 0.038	0.673 ± 0.038	0.674 ± 0.040
	BAO + HD	0.667 ± 0.036	0.721 ± 0.033	0.707 ± 0.055	0.736 ± 0.048	0.696 ± 0.019
	BAO + SN	0.681 ± 0.027	0.709 ± 0.024	0.674 ± 0.031	0.674 ± 0.031	0.703 ± 0.023
	BAO + HD + SN	0.680 ± 0.023	0.702 ± 0.020	0.676 ± 0.025	0.675 ± 0.023	0.697 ± 0.019
m_ϕ	HD	0.841 ± 0.524	...	1.780 ± 1.152	2.063 ± 1.062	
	SN	0.493 ± 0.311	...	1.000 ± 0.660	1.383 ± 0.675	
	BAO	0.664 ± 0.346	...	1.386 ± 0.867	1.636 ± 0.880	
	HD + SN	0.409 ± 0.241	...	0.852 ± 0.534	1.461 ± 0.814	
	BAO + HD	0.573 ± 0.326	...	1.514 ± 0.926	1.579 ± 0.864	
	BAO + SN	0.492 ± 0.195	...	0.971 ± 0.466	1.313 ± 0.553	
	BAO + HD + SN	0.473 ± 0.194	...	0.933 ± 0.443	1.305 ± 0.533	
m_ψ	HD	...	1.496 ± 0.846	1.662 ± 0.786	1.788 ± 0.751	
	SN	...	0.407 ± 0.307	0.713 ± 0.448	1.004 ± 0.515	
	BAO	...	0.635 ± 0.466	0.989 ± 0.534	1.354 ± 0.370	
	HD + SN	...	0.360 ± 0.243	0.628 ± 0.355	0.971 ± 0.360	
	BAO + HD	...	0.502 ± 0.364	1.014 ± 0.506	1.297 ± 0.260	
	BAO + SN	...	0.189 ± 0.140	0.601 ± 0.354	1.068 ± 0.247	
	BAO + HD + SN	...	0.191 ± 0.137	0.586 ± 0.350	1.067 ± 0.214	
β	HD	1.244 ± 5.413	
	SN	-3.120 ± 5.525	
	BAO	3.590 ± 3.504	
	HD + SN	1.041 ± 4.771	
	BAO + HD	4.344 ± 3.395	
	BAO + SN	0.382 ± 1.548	
	BAO + HD + SN	0.375 ± 1.476	
$-2 \ln \mathcal{L}_{\max}$	HD	6.11	5.40	4.87	4.39	6.11
	SN	1402.88	1403.12	1402.57	1397.92	1403.11
	BAO	9.06	9.45	7.80	7.34	9.46
	HD + SN	1409.13	1409.25	1409.13	1407.95	1409.23
	BAO + HD	15.63	15.87	14.15	13.41	15.87
	BAO + SN	1412.14	1414.97	1411.41	1411.43	1414.99
	BAO + HD + SN	1418.59	1421.4	1418.09	1418.11	1421.39
$\ln \mathcal{Z}$	HD	-8.75 ± 0.18	-7.67 ± 0.16	-7.76 ± 0.16	-8.31 ± 0.18	-7.76 ± 0.16
	SN	-707.47 ± 0.20	-707.57 ± 0.19	-708.01 ± 0.21	-708.82 ± 0.23	-706.05 ± 0.17
	BAO	-12.61 ± 0.23	-12.57 ± 0.22	-12.62 ± 0.23	-13.40 ± 0.24	-11.69 ± 0.21
	HD + SN	-712.61 ± 0.23	-712.61 ± 0.22	-713.22 ± 0.23	-714.57 ± 0.25	-711.10 ± 0.20
	BAO + HD	-16.01 ± 0.23	-16.29 ± 0.23	-16.21 ± 0.23	-16.98 ± 0.25	-15.25 ± 0.22
	BAO + SN	-715.48 ± 0.25	-717.12 ± 0.25	-716.18 ± 0.26	-717.95 ± 0.28	-714.81 ± 0.22
	BAO + HD + SN	-718.81 ± 0.25	-720.40 ± 0.25	-719.77 ± 0.26	-721.90 ± 0.29	-718.06 ± 0.22

(Table continued)

TABLE I. (Continued)

Parameter	Data sets	Quintessence	Phantom	Quintom	Quintom + β	Λ CDM
$\ln B_{m,\Lambda}$	HD	-0.99	0.09	0	-0.55	0
	SN	-1.42	-1.52	-1.96	-2.77	0
	BAO	-0.92	-0.88	-0.93	-1.71	0
	HD + SN	-1.51	-1.51	-2.12	-3.47	0
	BAO + HD	-0.76	-1.04	-0.96	-1.73	0
	BAO + SN	-0.67	-2.31	-1.37	-3.14	0
	BAO + HD + SN	-0.75	-2.34	-1.71	-3.84	0

all data sets and their combinations show that $\beta = 0$ is statistically admissible (the two-dimensional marginalized distributions of β and h are shown in the right panel of Fig. 6 for different combinations of data sets). Despite this fact, some important features come up with the introduction of this parameter. Some points to note concerning the quintom + β model are that, once again, the mass of the quintessence field is larger than the mass of the phantom field. This implies that, in this model as well, a preference exists for quintessence domination. It is also important to note that the masses of the fields are generally larger than those in the quintom model. In fact, for quintessence, all of them are greater than 1. In the right panel of Fig. 5 we show the constraints of the quintom + β model using BAO and additional data sets. A similar correlation occurs with the mass of the phantom and quintessence field (compared to the standard quintom model without coupling). This is an important point to stress because now the data sets are in favor of a m_ψ that is different from zero with more than 2σ CL; in fact, the tightest constraint yields $m_\psi = 1.067 \pm 0.214$ (BAO + HD + SN), which also yields higher values of the quintessence mass $m_\phi = 1.305 \pm 0.533$ (BAO + HD + SN). To have a closer look at the correlations among the

quintom + β parameters, the middle panel of Fig. 6 shows the two-dimensional marginalized posterior distributions of m_ϕ and m_ψ , color coded with β values. In this case, the most significant improvement to the fit occurs again when we consider the BAO + SN data set (with $-2 \ln \Delta \mathcal{L}_{\max} = 3.56$). However, the results for the BAO + SN + HD combination are very close ($-2 \ln \Delta \mathcal{L}_{\max} = 3.28$). The inclusion of this coupling produces a difference in favor of the model that contributes to diminishing the BAO tension created between low-redshift (galaxies) and high-redshift (Ly- α) data, as explored in [68,83]. Even though this model contains three extra parameters, the Bayes factor, with respect to Λ CDM, highlights this aspect by imposing a more significant penalty compared to all of the other models under consideration. However, this penalty is not high enough to discard the quintom + β model, as $|\Delta \ln \mathcal{Z}| \leq 3.84$. Specifically, the values of $|\Delta \ln \mathcal{Z}|$ indicate that when considering only HD data it is weakly disfavored; it is definitively disfavored for SN, BAO, and BAO + SN combinations, and strongly disfavored by HD + SN, BAO + SN, and BAO + HD + SN data set combinations. In a work in progress, for the quintom model with coupling, we are testing different potentials

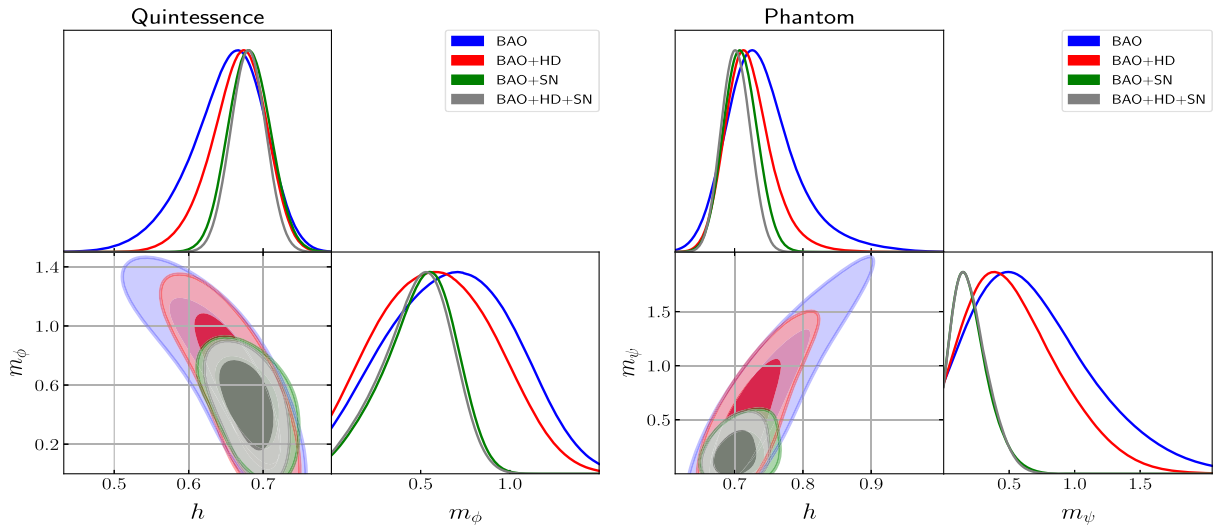


FIG. 4. One- and two-dimensional (68% and 95% CL) marginalized posterior distributions for the free parameters of quintessence (left) and phantom (right) dark energy models using BAO (blue), BAO + HD (red), BAO + SN (green), and BAO + HD + SN (gray).

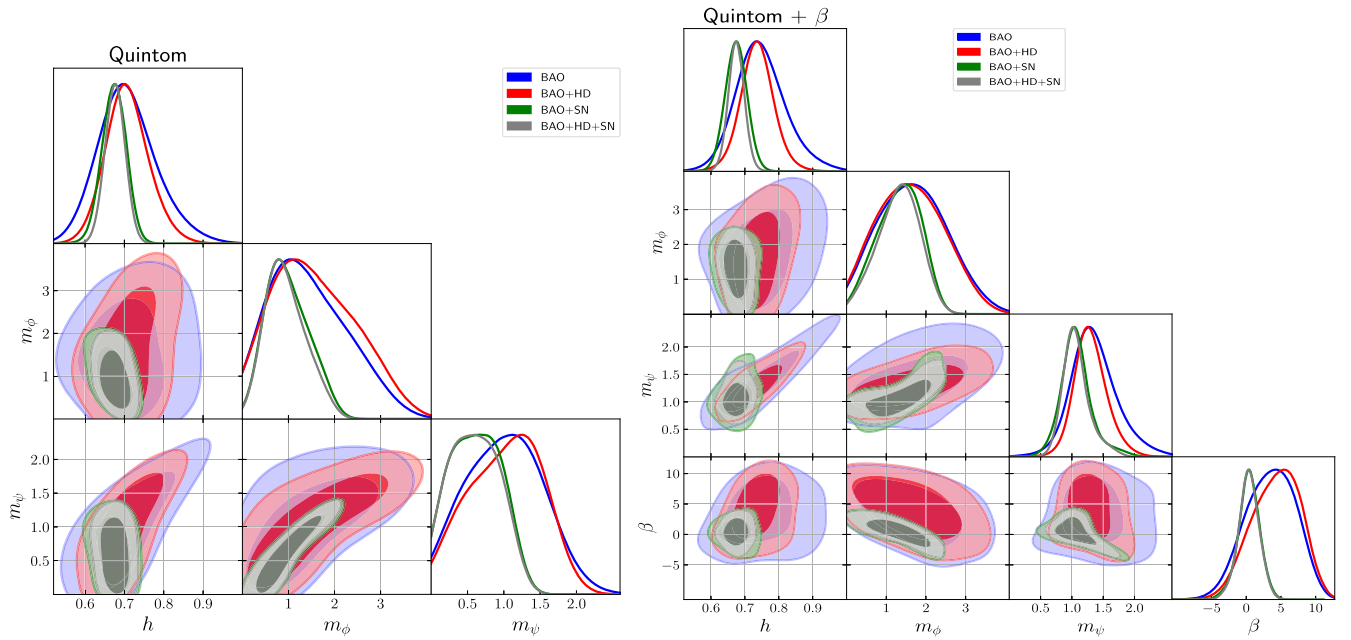


FIG. 5. One- and two-dimensional (68% and 95% CL) marginalized posterior distributions for the free parameters of quintom (left) and quintom + β (right) dark energy models using BAO (blue), BAO + HD (red), BAO + SN (green), and BAO + HD + SN (gray).

along with the *Planck* data set (including linear perturbations); however, for now, we are interested in the background cosmology.

Having performed the parameter estimation, we are able to plot some derived probability distribution functions in order to look at the locations of the main deviations from the Λ CDM model. For instance, the left panel of Fig. 7 displays the Hubble function $H(z)/(1+z)$ and the right panel shows the dark energy equation of state [Eq. (6)]. In this figure we present the results using BAO (top) and the

combined BAO + HD + SN data set (bottom), and also include the tip of the red-giant branch (TRGB) H_0 and BAO data points for comparison (red error bars). The solid lines represent the 1σ and 2σ CL and darker tones mean a better likelihood as shown in the color bar; for comparison, the dashed blue line corresponds to the Λ CDM prediction. We observe that there is a shift in the amplitude to lower values of $H(z)$, as is clear for the case of BAO where almost the entire 1σ region is lower than Λ CDM, and for the case of combined data this shift becomes small, as the

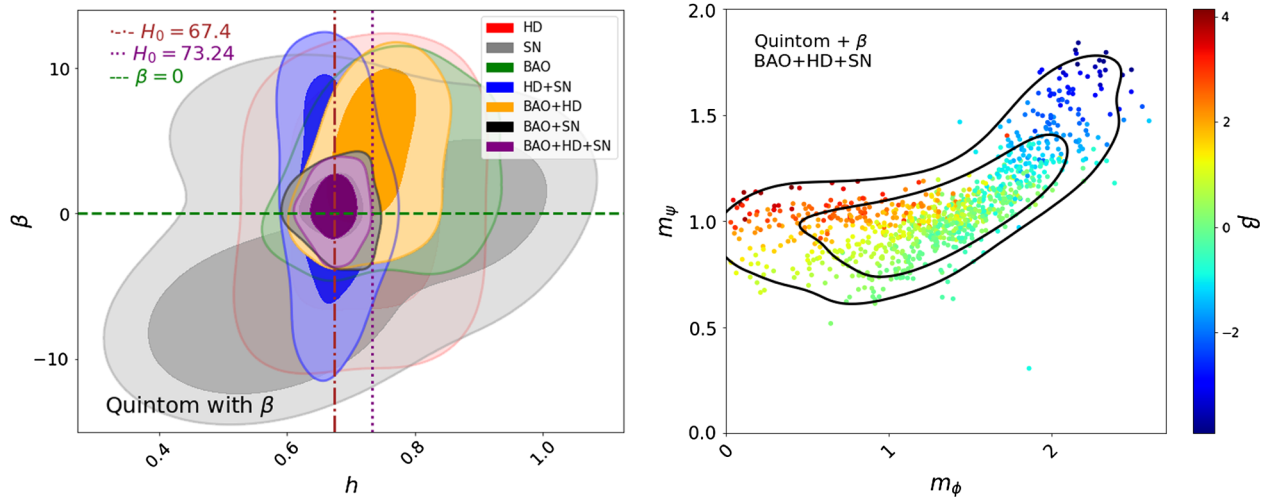


FIG. 6. Quintom + β model. Left: two-dimensional marginalized posterior distributions (68% and 95% CL) in the β - h plane for different combinations of data sets; the dashed lines correspond to the Λ CDM model: $H_0 = 73.24 \text{ km s}^{-1} \text{ Mpc}^{-1}$ coming from the Cepheid variables [89], and $H_0 = 67.40 \text{ km s}^{-1} \text{ Mpc}^{-1}$ measured by the *Planck* mission [90]. Right: scatter plot in the m_ϕ - m_ψ plane for different values of β (color bar), for BAO + HD + SN.

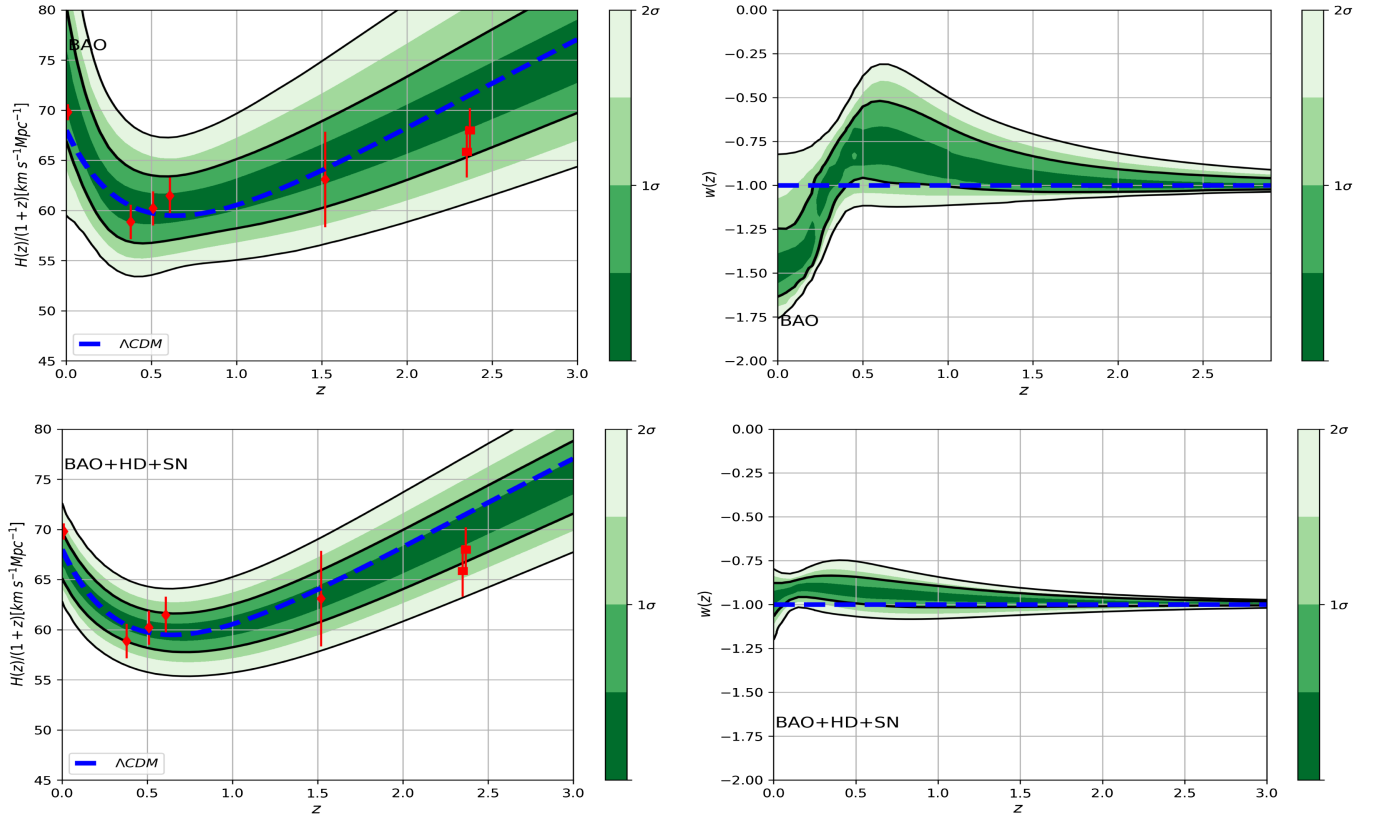


FIG. 7. Cosmological functions derived from the posterior distributions using the quintom + β model, showing $H(z)/(1+z)$ (left) and the EoS parameter $w(z)$ (right), using BAO (top) and BAO + HD + SN (bottom) data sets. The blue dashed lines represent the value of Λ CDM with the same parameter estimation as shown in Table I. The red error bars correspond to $H_0 = 69.8 \pm 0.8 \text{ km s}^{-1} \text{ Mpc}^{-1}$ from the TRGB [91], BAO galaxy consensus ($z \sim 0.5$) [56], BOSS DR14 quasars (eBOSS, $z = 1.52$) [92], and Ly- α DR16 and cross correlation ($z = 2.35$) and autocorrelation ($z = 2.37$) [87].

constraints increase. Regarding the effective dark energy EoS, its best-fit value at $z = 0$ is located below $w = -1$ (allowing small deviations in favor to the phantom region), and then it increases to cross the PDL and reaches a maximum value at about $z = 0.5$, where the BAO galaxy points are located [also observed as an inverted bump in $H(z)$ figure]. Notice that at this redshift the quintom + β model deviates by more than 2σ from the cosmological constant. After $w(z)$ has achieved the maximum value, it decreases to slightly cross back over the PDL again; this behaviour may be in favor to fit the BAO-Ly α as well. For the case of the joint data analysis we have a similar behavior but it is more constrained, with $w(z = 0) \approx -1.1$ with a more restricted range but also favoring the phantom region; the maximum is smaller too and throughout the redshift range $w = -1$ is acceptable. We must emphasize that the behavior presented by the EoS of the quintom + β model with the values obtained from observational constraints (right panel of Fig. 7) is qualitatively similar to that obtained from model-independent reconstructions [4,17–19], showing that the quintom model with coupling is a plausible option to model the most recent observational results of dark energy.

VI. CONCLUSIONS AND DISCUSSION

In this work, we have analyzed models of dark energy as minimally coupled scalar fields, specifically, a quintessence model and a phantom model with the quadratic potentials (11) and (12), a quintom model as the sum of the quadratic potentials of the previous two fields [Eq. (13)], and a novel proposal, dubbed quintom + β , with the sum of the quadratic potentials and the interaction term (14), inspired by [61]. Although the quintessence and phantom models with quadratic potentials, as well as the quintom model as the sum of these, have been well-known for some time, in order to make an update, in this work we constrained the parameters using late-time data. Our main focus was to study the new proposal quintom + β , which enriches the quintom model in a simple way by adding only one extra degree of freedom to the usual nonminimal quintom model (the simplest coupling between the quintessence and phantom fields). We showed that one of the main features of quintom + β is that it produces a wavelike EoS (see Fig. 3) similar to the one reported in other works in other contexts [72]. When constraining the parameters, quintom + β fits very well to the background cosmological data, especially for the SN data, which exhibits a preferred

negative β value and results in an improvement of $-\ln \Delta\mathcal{L}_{\max} = 5.19$ compared to Λ CDM. This result leads to an EoS that starts, at early times, slightly below -1 , then increases smoothly, peaking at $z \approx 0.5$, and then decreases to end up with a phantom value at the present time, $w(z=0) \approx -1.2$. Using the best-fit values, the CL for $H(z)$ and the EoS were calculated; the best fit of the parameters provides an EoS that is qualitatively similar to that reported by nonparametric reconstructions of dark energy [4] (see the top tight panel Fig. 7). As has already been said, this is precisely the behavior obtained from reconstructions, which allows us to say that quintom + β with only one additional parameter to the two necessarily associated with the quintessence field and phantom may reproduce the possible nature of the EoS obtained from observations. This makes the proposal of this work interesting, which motivates a more careful exploration of quintom models with potentials that couple the quintessence and phantom fields. It seems that interactions between fields through the product of powers of the fields, $V_{\text{int}} \propto \phi^n \psi^m$, may play an important role in describing the dynamics of dark energy and may be a more economical way to add dynamics (several crossings of the PDL) instead of potentials with elaborate functions with a vaguely clear justification.

For four scalar field dark energy models (quintessence, phantom, quintom, quintom + β) and for Λ CDM (for comparison), the cosmological and model parameters were constrained using HD, SN, and BAO data and their combinations, in addition to calculating the Bayesian evidence. The observational constraints of the quintessence and phantom potential parameters associated with the mass of the fields, m_ϕ and m_ψ , give values for both around $m_{\phi,\psi} \approx 0.2-1.5$ and with a slight correlation with h (m_ϕ directly proportional and m_ψ inversely proportional). For the quintom model, the parameters are also of the same order and slightly bigger than for the quintessence and phantom models, $m_{\phi,\psi} \approx 0.6-1.8$, but in this case without a correlation with h . For the proposed model quintom + β , the mass parameters are both $m_{\phi,\psi} \approx 1.0-2.06$ and the coupling parameter $\beta \approx -3.1-3.6$; it is noteworthy that in all cases the error bars of the constraints all cases the error bars of the constraints are of the order of the mass parameter values and even larger when included the β parameter. A natural improvement is to consider the CMB data and perform a more detailed study considering linear perturbations.

The proposal to model the dark energy with quintessence and phantom scalar fields (to allow PDL crossing) with a potential with an interacting term (to allow several crossings) seems to be reasonable since it is a flexible model that allows a dynamical EoS requiring three parameters (one for each field and one for the interaction) and with a simple functional form for the potential (polynomials). The quintom models are still valid as a candidate for dark energy; a

deeper and more careful study of the origin of scalar fields is needed as well as better observational constraints.

ACKNOWLEDGMENTS

J. A. V. acknowledges the support provided by FOSEC SEP-CONACYT Investigación Básica A1-S-21925, UNAM-DGAPA-PAPIIT IN117723, and FORDECYT-PRONACES-CONACYT/304001/2019. I. Q. acknowledges FORDECYT-PRONACES-CONACYT for support of the present research under grant CF-MG-2558591. A. A. S. acknowledges the funding from SERB, Govt of India under the Research Grant No CRG/2020/004347. I. G.-V. and G. G.-A. acknowledge the CONAHCYT post-doctoral fellowship and the support of the ICF-UNAM.

APPENDIX

The dynamics of quintom models with various potentials have also been explored using dynamical system techniques. One of the studied potentials consists of a sum of individual exponentials, without a direct coupling [93], and with a particular interaction potential between the phantom and quintessence fields [94]:

$$V = V_{\phi 0} e^{-\lambda_\phi \kappa \phi} + V_{\psi 0} e^{-\lambda_\psi \kappa \psi} + V_{\text{int}}(\phi, \psi). \quad (\text{A1})$$

For this potential, the authors found that there is a future attractor dominated by the phantom field, indicating an EoS below -1 at late times. Their analysis also showed that the Universe went through distinct stages that allowed the quintessence field to dominate ($w > -1$) in the past. This implies that the model enables a transition across the PDL irrespective of whether or not there is a direct coupling between the fields. In Ref. [93], it was shown that a similar EoS behavior to the one associated with Eq. (A1) can be achieved by Eq. (13). However, they showed that the sum of potentials with a quadratic scalar field in the exponents, given by

$$V = V_{\phi 0} e^{-\lambda_\phi \kappa^2 \phi^2} + V_{\psi 0} e^{-\lambda_\psi \kappa^2 \psi^2}, \quad (\text{A2})$$

leads to an opposite behavior where the EoS transitions from being below -1 (at early times) to above -1 and tends to approach -1 at late times; this is similar to our findings for the quintom + β with $\beta < 0$ [see Fig. 3(d)]. The EoS can also exhibit an oscillatory behavior. For instance, Fig. 8 shows some cases when varying the mass of the field for the oscillatory potential

$$V = m_\phi^2 (1 - \cos(a\phi)) + m_\psi^2 (1 - \cos(a\psi)). \quad (\text{A3})$$

Similar to the behavior of Eq. (A3), in Ref. [94], the authors argued that the following potentials can yield an oscillatory EoS where the oscillations across -1 can occur in the recent past and have the potential to produce observable effects:

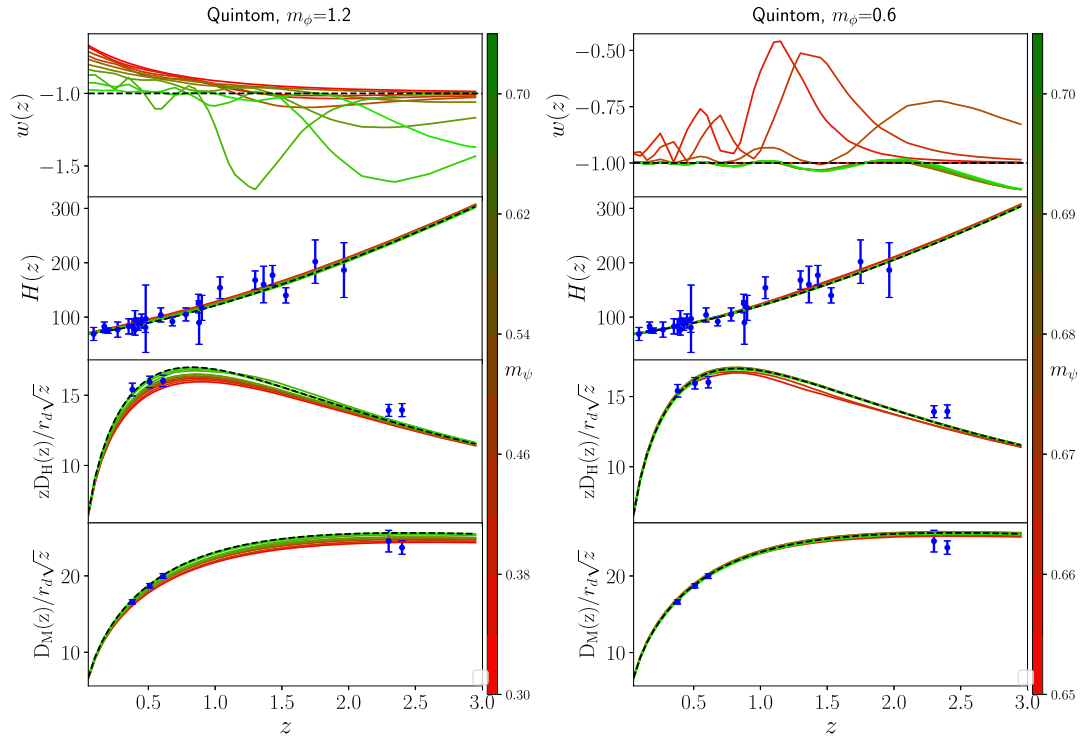


FIG. 8. Quintom model with an oscillatory potential. We show $w(z)$, $H(z)$, $D_H(z)$, and $D_M(z)$ for different values of the parameters m_ϕ for the oscillatory potential (A3).

$$V = V_1 \cos\left(\xi \frac{\phi}{M_P}\right) + V_2 \cos\left(\beta \frac{\phi}{M_P}\right) + \beta \phi^2 \psi^2, \quad (\text{A4})$$

$$V = \frac{1}{2} m_\phi^2 \phi^2 + \frac{1}{2} m_\psi^2 \psi^2 + \beta \psi^2 \phi^2. \quad (\text{A5})$$

Another combination of potentials that has been explored in the quintom scenario is the linear potential [95,96]:

$$V = a(\phi + \psi) + \beta \phi \psi. \quad (\text{A6})$$

By changing the sign of the coupling constant β , the model is capable of emulating the distinct characteristics exhibited by both quintessence and phantom models, similar to our findings.

-
- [1] Dragan Huterer and Daniel L. Shafer, Dark energy two decades after: Observables, probes, consistency tests, *Rep. Prog. Phys.* **81**, 016901 (2018).
- [2] Elcio Abdalla *et al.*, Cosmology intertwined: A review of the particle physics, astrophysics, and cosmology associated with the cosmological tensions and anomalies, *J. High Energy Astrophys.* **34**, 49 (2022).
- [3] Edmund J. Copeland, M. Sami, and Shinji Tsujikawa, Dynamics of dark energy, *Int. J. Mod. Phys. D* **15**, 1753 (2006).
- [4] Gong-Bo Zhao *et al.*, Dynamical dark energy in light of the latest observations, *Nat. Astron.* **1**, 627 (2017).
- [5] Joan Sola Peracaula, Adria Gomez-Valent, and Javier de Cruz Pérez, Signs of dynamical dark energy in current observations, *Phys. Dark Universe* **25**, 100311 (2019).
- [6] Deng Wang, Wei Zhang, and Xin-He Meng, Searching for the evidence of dynamical dark energy, *Eur. Phys. J. C* **79**, 1 (2019).
- [7] Anton Chudaykin, Konstantin Dolgikh, and Mikhail M. Ivanov, Constraints on the curvature of the Universe and dynamical dark energy from the full-shape and BAO data, *Phys. Rev. D* **103**, 023507 (2021).
- [8] Weiqiang Yang, Eleonora Di Valentino, Supriya Pan, Yabo Wu, and Jianbo Lu, Dynamical dark energy after Planck CMB final release and H_0 tension, *Mon. Not. R. Astron. Soc.* **501**, 5845 (2021).
- [9] Eleonora Di Valentino, Olga Mena, Supriya Pan, Luca Visinelli, Weiqiang Yang, Alessandro Melchiorri, David F. Mota, Adam G. Riess, and Joseph Silk, In the realm of the

- Hubble tension—A review of solutions, *Classical Quantum Gravity* **38**, 153001 (2021).
- [10] Sebastian Bahamonde, Christian G. Böhrer, Sante Carloni, Edmund J. Copeland, Wei Fang, and Nicola Tamanini, Dynamical systems applied to cosmology: Dark energy and modified gravity, *Phys. Rep.* **775–777**, 1 (2018).
- [11] Israel Quiros, Selected topics in scalar–tensor theories and beyond, *Int. J. Mod. Phys. D* **28**, 1930012 (2019).
- [12] Shinji Tsujikawa, Quintessence: A review, *Classical Quantum Gravity* **30**, 214003 (2013).
- [13] Kevin J. Ludwick, The viability of phantom dark energy: A review, *Mod. Phys. Lett. A* **32**, 1730025 (2017).
- [14] Luis P. Chimento, Ruth Lazkoz, Roy Maartens, and Israel Quiros, Crossing the phantom divide without phantom matter, *J. Cosmol. Astropart. Phys.* **09** (2006) 004.
- [15] Yi-Fu Cai, Emmanuel N. Saridakis, Mohammad R. Setare, and Jun-Qing Xia, Quintom cosmology: Theoretical implications and observations, *Phys. Rep.* **493**, 1 (2010).
- [16] Luis A. Escamilla and J. Alberto Vazquez, Model selection applied to reconstructions of the dark energy, *Eur. Phys. J. C* **83**, 251 (2023).
- [17] J. Alberto Vazquez, M. Bridges, M. P. Hobson, and A. N. Lasenby, Reconstruction of the dark energy equation of state, *J. Cosmol. Astropart. Phys.* **09** (2012) 020.
- [18] S. Hee, J. A. Vázquez, W. J. Handley, M. P. Hobson, and A. N. Lasenby, Constraining the dark energy equation of state using Bayes theorem and the Kullback–Leibler divergence, *Mon. Not. R. Astron. Soc.* **466**, 369 (2017).
- [19] Yuting Wang, Levon Pogossian, Gong-Bo Zhao, and Alex Zucca, Evolution of dark energy reconstructed from the latest observations, *Astrophys. J. Lett.* **869**, L8 (2018).
- [20] Sirachak Panpanich, Piyabut Burikham, Supakchai Ponglertsakul, and Luchakorn Tannukij, Resolving Hubble tension with quintom dark energy model, *Chin. Phys. C* **45**, 015108 (2021).
- [21] Ji-Ping Dai, Yang Yang, and Jun-Qing Xia, Reconstruction of the dark energy equation of state from the latest observations, *Astrophys. J.* **857**, 9 (2018).
- [22] Wayne Hu, Crossing the phantom divide: Dark energy internal degrees of freedom, *Phys. Rev. D* **71**, 047301 (2005).
- [23] Bo Feng, Xiulian Wang, and Xinmin Zhang, Dark energy constraints from the cosmic age and supernova, *Phys. Lett. B* **607**, 35 (2005).
- [24] Y.F. Cai, E.N. Saridakis, M.R. Setare, and J.Q. Xia, Quintom cosmology: Theoretical implications and observations, *Phys. Rep.* **493**, 1 (2010).
- [25] Taotao Qiu, Theoretical aspects of quintom models, *Mod. Phys. Lett. A* **25**, 909 (2010).
- [26] Ming-Jian Zhang and Hong Li, Observational constraint on the dark energy scalar field, *Chin. Phys. C* **45**, 045103 (2021).
- [27] Ruth Lazkoz, Genly Leon, and Israel Quiros, Quintom cosmologies with arbitrary potentials, *Phys. Lett. B* **649**, 103 (2007).
- [28] Genly Leon, Andronikos Paliathanasis, and Jorge Luis Morales-Martínez, The past and future dynamics of quintom dark energy models, *Eur. Phys. J. C* **78**, 1 (2018).
- [29] Sudip Mishra and Subenoy Chakraborty, Dynamical system analysis of quintom dark energy model, *Eur. Phys. J. C* **78**, 917 (2018).
- [30] Mihai Marciu, Quintom dark energy with nonminimal coupling, *Phys. Rev. D* **93**, 123006 (2016).
- [31] J. Socorro, Priscila Romero, Luis O. Pimentel, and M. Aguero, Quintom potentials from quantum cosmology using the FRW cosmological model, *Int. J. Theor. Phys.* **52**, 2722 (2013).
- [32] Sourav Dutta, Muthusamy Lakshmanan, and Subenoy Chakraborty, Quantum cosmology with symmetry analysis for quintom dark energy model, *Phys. Dark Universe* **32**, 100795 (2021).
- [33] J. Alberto Vázquez, David Tamayo, Anjan A. Sen, and Israel Quiros, Bayesian model selection on scalar ϵ -field dark energy, *Phys. Rev. D* **103**, 043506 (2021).
- [34] David Benisty and Eduardo I. Guendelman, Two scalar fields inflation from scale-invariant gravity with modified measure, *Classical Quantum Gravity* **36**, 095001 (2019).
- [35] Atalia Navarro-Boullosa, Argelia Bernal, and J. Alberto Vazquez, Bayesian analysis for rotational curves with ℓ -boson stars as a dark matter component, *J. Cosmol. Astropart. Phys.* **09** (2023) 031.
- [36] L. O. Téllez-Tovar, Tonatiuh Matos, and J. Alberto Vázquez, Cosmological constraints on the multiscalar field dark matter model, *Phys. Rev. D* **106**, 123501 (2022).
- [37] Luis E. Padilla, J. Alberto Vázquez, Tonatiuh Matos, and Gabriel Germán, Scalar field dark matter spectator during inflation: The effect of self-interaction, *J. Cosmol. Astropart. Phys.* **05** (2019) 056.
- [38] David Benisty and Eduardo I. Guendelman, Two scalar fields inflation from scale-invariant gravity with modified measure, *Classical Quantum Gravity* **36**, 095001 (2019).
- [39] Kazuharu Bamba, Sergei D. Odintsov, and Petr V. Tretyakov, Inflation in a conformally-invariant two-scalar-field theory with an extra R^2 term, *Eur. Phys. J. C* **75**, 344 (2015).
- [40] J. Alberto Vázquez, Luis E. Padilla, and Tonatiuh Matos, Inflationary cosmology: From theory to observations, *Rev. Mex. Fis. E* **17**, 73 (2020).
- [41] Orfeu Bertolami, Pedro Carrilho, and Jorge Páramos, Two-scalar-field model for the interaction of dark energy and dark matter, *Phys. Rev. D* **86**, 103522 (2012).
- [42] Asimina Arvanitaki, Savas Dimopoulos, Sergei Dubovsky, Nemanja Kaloper, and John March-Russell, String axiverse, *Phys. Rev. D* **81**, 123530 (2010).
- [43] Viraf M. Mehta, Mehmet Demirtas, Cody Long, David J. E. Marsh, Liam McAllister, and Matthew J. Stott, Super-radiance in string theory, *J. Cosmol. Astropart. Phys.* **07** (2021) 033.
- [44] Michele Cicoli, Veronica Guidetti, Nicole Righi, and Alexander Westphal, Fuzzy dark matter candidates from string theory, *J. High Energy Phys.* **05** (2022) 001.
- [45] Eréndira Gutiérrez-Luna, Belen Carvente, Víctor Jaramillo, Juan Barranco, Celia Escamilla-Rivera, Catalina Espinoza, Myriam Mondragón, and Darío Núñez, Scalar field dark matter with two components: Combined approach from particle physics and cosmology, *Phys. Rev. D* **105**, 083533 (2022).
- [46] Bo Feng, Mingzhe Li, Yun-Song Piao, and Xinmin Zhang, Oscillating quintom and the recurrent universe, *Phys. Lett. B* **634**, 101 (2006).

- [47] Yi-Fu Cai, Hong Li, Yun-Song Piao, and Xin-min Zhang, Cosmic duality in quintom universe, *Phys. Lett. B* **646**, 141 (2007).
- [48] Raul Jimenez, Licia Verde, Tommaso Treu, and Daniel Stern, Constraints on the equation of state of dark energy and the Hubble constant from stellar ages and the cosmic microwave background, *Astrophys. J.* **593**, 622 (2003).
- [49] Joan Simon, Licia Verde, and Raul Jimenez, Constraints on the redshift dependence of the dark energy potential, *Phys. Rev. D* **71**, 123001 (2005).
- [50] Daniel Stern, Raul Jimenez, Licia Verde, Marc Kamionkowski, and S Adam Stanford, Cosmic chronometers: Constraining the equation of state of dark energy. I: $h(z)$ measurements, *J. Cosmol. Astropart. Phys.* **02** (2010) 008.
- [51] Michele Moresco, Licia Verde, Lucia Pozzetti, Raul Jimenez, and Andrea Cimatti, New constraints on cosmological parameters and neutrino properties using the expansion rate of the universe to $z \sim 1.75$, *J. Cosmol. Astropart. Phys.* **07** (2012) 053.
- [52] Cong Zhang, Han Zhang, Shuo Yuan, Siqi Liu, Tong-Jie Zhang, and Yan-Chun Sun, Four new observational $h(z)$ data from luminous red galaxies in the Sloan Digital Sky Survey data release seven, *Res. Astron. Astrophys.* **14**, 1221 (2014).
- [53] Michele Moresco, Raising the bar: New constraints on the Hubble parameter with cosmic chronometers at $z \sim 2$, *Mon. Not. R. Astron. Soc.* **450**, L16 (2015).
- [54] Michele Moresco, Lucia Pozzetti, Andrea Cimatti, Raul Jimenez, Claudia Maraston, Licia Verde, Daniel Thomas, Annalisa Citro, Rita Tojeiro, and David Wilkinson, A 6% measurement of the Hubble parameter at $z \sim 0.45$: Direct evidence of the epoch of cosmic re-acceleration, *J. Cosmol. Astropart. Phys.* **05** (2016) 014.
- [55] A. L. Ratsimbazafy, S. I. Loubser, S. M. Crawford, C. M. Cress, B. A. Bassett, R. C. Nichol, and P. Väisänen, Age-dating luminous red galaxies observed with the Southern African Large Telescope, *Mon. Not. R. Astron. Soc.* **467**, 3239 (2017).
- [56] Shadab Alam, Metin Ata, Stephen Bailey, Florian Beutler, Dmitry Bizyaev, Jonathan A. Blazek, Adam S. Bolton, Joel R. Brownstein, Angela Burden, Chia-Hsun Chuang *et al.*, The clustering of galaxies in the completed SDSS-III baryon oscillation spectroscopic survey: Cosmological analysis of the DR12 galaxy sample, *Mon. Not. R. Astron. Soc.* **470**, 2617 (2017).
- [57] Victoria de Sainte Agathe, Christophe Balland, Hélion Du Mas Des Bourbonx, Michael Blomqvist, Julien Guy, James Rich, Andreu Font-Ribera, Matthew M Pieri, Julian E. Bautista, Kyle Dawson *et al.*, Baryon acoustic oscillations at $z = 2.34$ from the correlations of $L\alpha$ absorption in eBOSS DR14, *Astron. Astrophys.* **629**, A85 (2019).
- [58] Michael Blomqvist, Hélion Du Mas Des Bourbonx, Victoria de Sainte Agathe, James Rich, Christophe Balland, Julian E. Bautista, Kyle Dawson, Andreu Font-Ribera, Julien Guy, Jean-Marc Le Goff *et al.*, Baryon acoustic oscillations from the cross-correlation of $L\alpha$ absorption and quasars in eBOSS DR14, *Astron. Astrophys.* **629**, A86 (2019).
- [59] H. H. Xiong Xiong, Y. F. Cai, T. Qiu, Y. S. Piao, and X. Zhang, Oscillating universe with quintom matter, *Phys. Lett. B* **666**, 212 (2008).
- [60] José Germán Salazar Arias, Fenomenología del modelo cosmológico SO(1,1), <https://repositorio.cinvestav.mx/bitstream/handle/cinvestav/3598/SSIT0016691.pdf?sequence=1> (2020).
- [61] Abdel Pérez-Lorenzana, Merced Montesinos, and Tonatiuh Matos, Unification of cosmological scalar fields, *Phys. Rev. D* **77**, 063507 (2008).
- [62] Yi-Fu Cai and Emmanuel N. Saridakis, Non-singular cyclic cosmology without phantom menace, *J. Cosmol.* **17**, 7238 (2011).
- [63] Sean M. Carroll, Mark Hoffman, and Mark Trodden, Can the dark energy equation-of-state parameter w be less than -1 ?, *Phys. Rev. D* **68**, 023509 (2003).
- [64] James M. Cline, Sangyong Jeon, and Guy D. Moore, The Phantom menaced: Constraints on low-energy effective ghosts, *Phys. Rev. D* **70**, 043543 (2004).
- [65] Özgür Akarsu, John D. Barrow, Charles V. R. Board, N. Merve Uzun, and J. Alberto Vazquez, Screening Λ in a new modified gravity model, *Eur. Phys. J. C* **79**, 846 (2019).
- [66] Rodrigo Calderón, Radouane Gannouji, Benjamin L'Huillier, and David Polarski, Negative cosmological constant in the dark sector?, *Phys. Rev. D* **103**, 023526 (2021).
- [67] Giovanni Acquaviva, Özgür Akarsu, Nihan Katirci, and J. Alberto Vazquez, Simple-graduated dark energy and spatial curvature, *Phys. Rev. D* **104**, 023505 (2021).
- [68] Özgür Akarsu, John D. Barrow, Luis A. Escamilla, and J. Alberto Vazquez, Graduated dark energy: Observational hints of a spontaneous sign switch in the cosmological constant, *Phys. Rev. D* **101**, 063528 (2020).
- [69] Özgür Akarsu, Suresh Kumar, Emre Özüiker, and J. Alberto Vazquez, Relaxing cosmological tensions with a sign switching cosmological constant, *Phys. Rev. D* **104**, 123512 (2021).
- [70] Anjan A. Sen, Shahnawaz A. Adil, and Somasri Sen, Do cosmological observations allow a negative Λ ?, *Mon. Not. R. Astron. Soc.* **518**, 1098 (2022).
- [71] Mohammad Malekjani, Ruairí Mc. Conville, Eoin Ó. Colgáin, Saeed Pourojaghi, and M. M. Sheikh-Jabbari, Negative dark energy density from high redshift Pantheon + Supernovae, [arXiv:2301.12725](https://arxiv.org/abs/2301.12725).
- [72] David Tamayo and J. Alberto Vazquez, Fourier-series expansion of the dark-energy equation of state, *Mon. Not. R. Astron. Soc.* **487**, 729 (2019).
- [73] Varun Sahni and Yuri Shtanov, Did the universe loiter at high redshifts?, *Phys. Rev. D* **71**, 084018 (2005).
- [74] Shinji Tsujikawa, Kotub Uddin, Shuntaro Mizuno, Reza Tavakol, and Jun'ichi Yokoyama, Constraints on scalar-tensor models of dark energy from observational and local gravity tests, *Phys. Rev. D* **77**, 103009 (2008).
- [75] Florian Bauer, Joan Sola, and Hrvoje Stefancic, Dynamically avoiding fine-tuning the cosmological constant: The 'Relaxed Universe', *J. Cosmol. Astropart. Phys.* **12** (2010) 029.
- [76] Varun Sahni, Arman Shafieloo, and Alexei A. Starobinsky, Model independent evidence for dark energy evolution from baryon acoustic oscillations, *Astrophys. J. Lett.* **793**, L40 (2014).

- [77] Adria Gomez-Valent, Elahe Karimkhani, and Joan Sola, Background history and cosmic perturbations for a general system of self-conserved dynamical dark energy and matter, *J. Cosmol. Astropart. Phys.* **12** (2015) 048.
- [78] Emre Ozulker, Is the dark energy equation of state parameter singular?, *Phys. Rev. D* **106**, 063509 (2022).
- [79] Shah Nawaz A. Adil, Özgür Akarsu, Eleonora Di Valentino, Rafael C. Nunes, Emre Özulker, Anjan A. Sen, and Enrico Specogna, Omnipotent dark energy: A phenomenological answer to the Hubble tension, [arXiv:2306.08046](https://arxiv.org/abs/2306.08046).
- [80] J. P. Petit and G. d'Agostini, Negative mass hypothesis in cosmology and the nature of dark energy, *Astrophys. Space Sci.* **354**, 2106 (2014).
- [81] Luca Visinelli, Sunny Vagnozzi, and Ulf Danielsson, Revisiting a negative cosmological constant from low-redshift data, *Symmetry* **11**, 1035 (2019).
- [82] J. A. Vazquez, I. Gomez-Vargas, and A. Slosar, Updated version of a simple MCMC code for cosmological parameter estimation where only expansion history matters, <https://github.com/ja-vazquez/SimpleMC> (2021).
- [83] Éric Aubourg, Stephen Bailey, Julian E. Bautista, Florian Beutler, Vaishali Bhardwaj, Dmitry Bizyaev, Michael Blanton, Michael Blomqvist, Adam S. Bolton, Jo Bovy *et al.*, Cosmological implications of baryon acoustic oscillation measurements, *Phys. Rev. D* **92**, 123516 (2015).
- [84] Luis E. Padilla, Luis O. Tellez, Luis A. Escamilla, and Jose Alberto Vazquez, Cosmological parameter inference with Bayesian statistics, *Universe* **7**, 213 (2021).
- [85] Michele Moresco, Raul Jimenez, Licia Verde, Andrea Cimatti, and Lucia Pozzetti, Setting the stage for cosmic chronometers. II. Impact of stellar population synthesis models systematics and full covariance matrix, *Astrophys. J.* **898**, 82 (2020).
- [86] Dillon Brout, Dan Scolnic, Brodie Popovic, Adam G. Riess, Anthony Carr, Joe Zuntz, Rick Kessler, Tamara M. Davis, Samuel Hinton, David Jones *et al.*, The pantheon + analysis: Cosmological constraints, *Astrophys. J.* **938**, 110 (2022).
- [87] Shadab Alam *et al.*, Completed SDSS-IV extended Baryon Oscillation Spectroscopic Survey: Cosmological implications from two decades of spectroscopic surveys at the Apache Point Observatory, *Phys. Rev. D* **103**, 083533 (2021).
- [88] Joshua S. Speagle, DYNESTY: A dynamic nested sampling package for estimating Bayesian posteriors and evidences, *Mon. Not. R. Astron. Soc.* **493**, 3132 (2020).
- [89] Adam G. Riess, Lucas M. Macri, Samantha L. Hoffmann, Dan Scolnic, Stefano Casertano, Alexei V. Filippenko, Brad E. Tucker, Mark J. Reid, David O. Jones, Jeffrey M. Silverman *et al.*, A 2.4% determination of the local value of the Hubble constant, *Astrophys. J.* **826**, 56 (2016).
- [90] Nabila Aghanim, Yashar Akrami, M. Ashdown, J. Aumont, C. Baccigalupi, M. Ballardini, A. J. Banday, R. B. Barreiro, N. Bartolo, S. Basak *et al.*, Planck 2018 results-VI. Cosmological parameters, *Astron. Astrophys.* **641**, A6 (2020).
- [91] Wendy L. Freedman, Barry F. Madore, Dylan Hatt, Taylor J. Hoyt, In Sung Jang, Rachael L. Beaton, Christopher R. Burns, Myung Gyoon Lee, Andrew J. Monson, Jillian R. Neeley *et al.*, The Carnegie-Chicago Hubble program. VIII. An independent determination of the Hubble constant based on the tip of the red giant branch, *Astrophys. J.* **882**, 34 (2019).
- [92] Metin Ata, Falk Baumgarten, Julian Bautista, Florian Beutler, Dmitry Bizyaev, Michael R. Blanton, Jonathan A. Blazek, Adam S. Bolton, Jonathan Brinkmann, Joel R. Brownstein *et al.*, The clustering of the SDSS-IV extended baryon oscillation spectroscopic survey DR14 quasar sample: First measurement of baryon acoustic oscillations between redshift 0.8 and 2.2, *Mon. Not. R. Astron. Soc.* **473**, 4773 (2018).
- [93] Zong-Kuan Guo, Yun-Song Piao, Xinmin Zhang, and Yuan-Zhong Zhang, Cosmological evolution of a quintom model of dark energy, *Phys. Lett. B* **608**, 177 (2005).
- [94] Xiao-Fei Zhang, Hong Li, Yun-Song Piao, and Xinmin Zhang, Two-field models of dark energy with equation of state across-1, *Mod. Phys. Lett. A* **21**, 231 (2006).
- [95] Leandros Perivolaropoulos, Constraints on linear negative potentials in quintessence and phantom models from recent supernova data, *Phys. Rev. D* **71**, 063503 (2005).
- [96] Puxun Wu and Hongwei Yu, Statefinder parameters for quintom dark energy model, *Int. J. Mod. Phys. D* **14**, 1873 (2005).